Journal of Power Sources 196 (2011) 8656–8661

Contents lists available at ScienceDirect

Journal of Power Sources

journal homepage: www.elsevier.com/locate/jpowsour

Improved cycle life of Fe-substituted $LiCoPO_4$

J.L. Allen*, T.R. Jow, J. Wolfenstine

U.S. Army Research Laboratory, 2800 Powder Mill Road, Adelphi, MD 20783-1197, USA

ARTICLE INFO

Article history:
Received 17 May 2011
Received in revised form 14 June 2011
Accepted 15 June 2011
Available online 22 June 2011

Keywords:
Li-ion battery
High voltage
XRD
Mössbauer
Cathode
$LiCoPO_4$

ABSTRACT

Fe-substituted $LiCoPO_4$ exhibits greatly improved cycle life relative to $LiCoPO_4$. Whereas, pure $LiCoPO_4$ loses more than half of its discharge capacity at the 10th cycle, the Fe-substituted $LiCoPO_4$ retains about 100% of its discharge capacity at the 10th cycle and about 80% of its capacity at the 500th cycle. It is suggested that improved cycle life results from Fe^{3+} substitution on the Li and Co sites. The partial substitution of Li^+ by Fe^{3+} and Co^{2+} by Fe^{2+} and Fe^{3+} was evidenced from Rietveld analysis of X-ray powder diffraction data, infrared spectroscopy, X-ray photoelectron spectroscopy and Mössbauer spectroscopy. The majority of the Fe^{3+} substitutes at the Co^{2+} site. The composition of Fe-substituted $LiCoPO_4$ is $Li_{0.92}Co_{0.8}Fe^{2+}_{0.12}Fe^{3+}_{0.08}PO_4$ for a sample of starting composition $LiCo_{0.8}Fe_{0.2}PO_4$.

Published by Elsevier B.V.

1. Introduction

$LiMPO_4$ compounds, where M = Fe, Mn, Co or Ni, have been the focus of intense study both for scientific and practical reasons as Li-ion battery energy storage materials since the pioneering work of Padhi et al. [1]. The voltage of the redox couple varies with transition metal from 3.4 V for Fe [1], 4.1 V for Mn [1], 4.8 V for Co [2] and 5.1 V for Ni [3]. High voltage batteries are desirable because the stored energy is proportional to the voltage and the power is proportional to the square of the voltage. For example, $LiFePO_4$ has potentially an energy storage capability of 578 W h kg^{-1} (3.4 V × 170 Ah kg^{-1}) and $LiCoPO_4$ about 802 W h kg^{-1} (4.8 V × 167 Ah kg^{-1}). Hence, there is a keen interest to move beyond already commercialized $LiFePO_4$ to the other transition metals. As $LiCoPO_4$ in particular has the potential to increase energy ~40% compared to $LiFePO_4$, we have focused our work on this material. Initial work on $LiCoPO_4$ led to improved rate capability but capacity fade soon emerged as an impediment to further progress [4–6]. The initial discharge capacity and rate capability of $LiCoPO_4$ were improved by varying the oxygen partial pressure during synthesis [6], carbon coating [7] and substitution on the Co site [8]. However, until now, $LiCoPO_4$ has shown a severe loss of discharge capacity upon charge–discharge cycling. For example, Tadanga et al. [4] observed a 10th cycle discharge capacity of ~52% of the initial capacity, Bramnik et al. [5] reported a 10th cycle discharge of ~59% of the initial capacity and Wolfenstine et al. [6] reported ~53% capacity retention at the 10th cycle. This capacity fade has been attributed to irreversible structural changes such as amorphization [5,6] of the material and/or electrolyte degradation [4]. In this paper, we will show that a substitution of Li^+ by Fe^{3+} and Co^{2+} by Fe^{3+} and Fe^{2+} improves not only rate capability but also dramatically reduces capacity fade. In addition, even further reduction in capacity fade is observed when the Fe-substituted $LiCoPO_4$ was used with electrolyte containing tris(hexafluoroisopropyl) phosphate (HFiP) [9].

2. Experimental

$LiCoPO_4$ samples were prepared via a citrate complexation route. $Co(OH)_2$, LiH_2PO_4, and citric acid, 1, 1.01, 1.02, molar ratio, respectively, were mixed into deionized water until all solids were dissolved. The resulting solution was evaporated to dryness via a microwave oven. The resulting dried mass was removed, ground lightly with mortar and pestle and heated in air at a rate of 10 °C min^{-1} to 600 °C and the reactant mixture was held at this temperature for 12 h.

In order get Fe substitution on both the Li and Co sites, $Co(OH)_2$, LiH_2PO_4 and $FeC_2O_4{\cdot}2H_2O$ with a nominal stoichiometry of $LiCo_{1-x}Fe_xPO_4$, $x = 0.05, 0.1, 0.2$ were weighed and then dissolved in 1 M HNO_3 (aq). The resulting nitrate solution was evaporated to dryness via a microwave oven in a fume hood and then heated under N_2 at a rate of 10 °C min^{-1} to 600 °C and held at this temperature for 12 h. During the decomposition of the co-precipitated nitrates, the decomposition of the nitrate ion provided an oxidizing

* Corresponding author. Tel.: +1 301 394 0291; fax: +1 301 394 0273.
E-mail addresses: jan.l.allen8.civ@mail.mil, jallen@arl.army.mil (J.L. Allen).

0378-7753/$ – see front matter. Published by Elsevier B.V.
doi:10.1016/j.jpowsour.2011.06.057

component to the N_2 atmosphere which transformed a portion of the Fe^{2+} to Fe^{3+}.

Carbon coating to improve electronic conductivity was done by ball milling the samples of $LiCoPO_4$ and Fe-substituted $LiCoPO_4$ for 30 min with 5% by mass acetylene black followed by heating for 1 h at 600 °C under N_2. The improvements of the activity of $LiCoPO_4$ after carbon coating [5] and after a short ball milling (<1 h) have been previously reported [10].

Phase purity was evaluated using X-ray powder diffraction. Data were collected using a Rigaku Ultima III diffractometer. Lattice constants were calculated from peak positions using Rietveld refinement of the pattern collected in a parallel beam geometry or with the use of a NIST certified silicon standard for collection in a Bragg–Brentano geometry using Riqas software (Materials Data Inc.). Samples were further evaluated spectroscopically using Attenuated Total Reflectance Fourier-Transform Infrared (ATR-FTIR) Spectroscopy, X-ray Photoelectron Spectroscopy (XPS) to evaluate site occupancy and oxidation states, respectively. Additional information about the oxidation state of Fe was obtained from Mössbauer spectroscopy (collected at SEE Company, Edina, Mn) and elemental analysis via inductively coupled plasma optical emission spectroscopy (ICP-OES, data collected at Galbraith Laboratories, Inc.).

For electrochemical testing, a composite electrode was fabricated by a slurry coating method. Using N-methylpyrrolidone (NMP) as solvent, a slurry was used to coat an Al foil substrate to produce a composite electrode of 80 wt.% active, 10 wt.% polyvinylidene fluoride (PVDF) and 8 wt.% super-P carbon and 2 wt.% conductive carbon nanotube composite (CheapTubes.com). The electrode film was cut into small discs with an area of 0.97 cm^2, dried under an infrared lamp in air before use and thereafter in a heated vacuum oven (~100 °C). In a dry room (dew point < −80 °C), Li/active coin cells (Hohsen Al-clad CR2032) were assembled using Celgard® 3501 as the separator and a 1.0 molal $LiPF_6$ solution in a 3:7 (wt.%) mixture of ethylene carbonate (EC) and ethyl methyl carbonate (EMC) electrolyte with and without 1 wt.% HFiP. Electrochemical testing was performed using a Maccor Series 4000 tester. For calculation of C-rate, a capacity of ~170 mA h g^{-1} was assumed.

3. Results and discussion

The partial substitution of Co^{2+} by Fe^{2+} was explored because is known that substitution with Fe^{2+} can improve the rate capability of the other olivines [1]. For example, Padhi et al. [1] showed that Fe substitution for Mn^{2+} in $LiMnPO_4$ enabled it to be cycled whereas pure $LiMnPO_4$ was found to be essentially electrochemically inert. At the time, Padhi et al. proposed that the Fe^{3+}–O–Mn^{2+} interactions destabilize the Mn^{2+} level and stabilize the Fe^{3+} level so as to make the Mn^{3+}/Mn^{2+} energy accessible. Thus, we report here on the substitution of Co^{2+} by Fe^{2+} as a means to improve the rate capability in an analogous fashion. However, there is no reported improvement in capacity fade owing to the substitution of Co^{2+} by Fe^{2+}.

The partial substitution of Li^+ and Co^{2+} by Fe^{3+} was explored to address capacity fade through improved structural stability of $LiCoPO_4/CoPO_4$ during cycling. This substitutional strategy is based upon the speculation that decomposition of $LiCoPO_4$ or $CoPO_4$ may result from a loss of oxygen during charging–discharging as shown below.

For the case of $CoPO_4$, the proposed decomposition reaction is:

$$2CoPO_4 \rightarrow Co_2P_2O_7 + 1/2O_2 \quad (1)$$

This reaction results in the release of O_2 during the discharge. This potential mechanism is proposed based on the reported decomposition of $CoPO_4$ to $Co_2P_2O_7$ and O_2 during heating under reducing conditions [11].

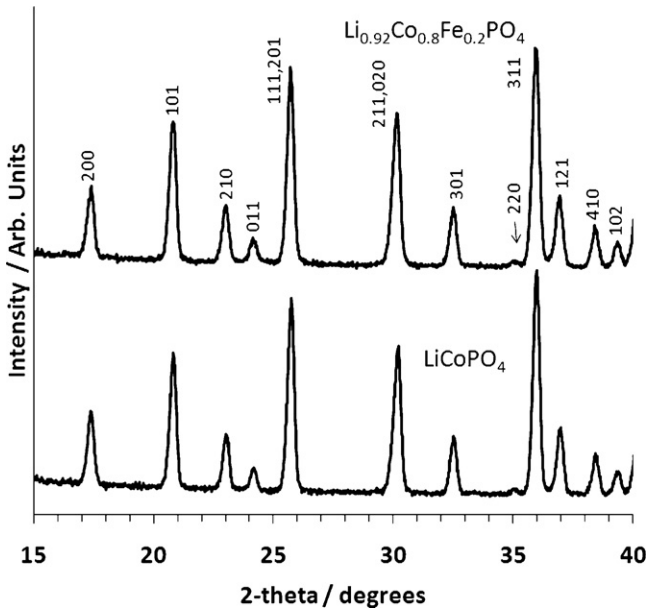

Fig. 1. X-ray powder diffraction pattern of $LiCoPO_4$ prepared via citrate aqueous precursor route, bottom, and the X-ray powder diffraction pattern of $Li_{0.92}Co_{0.8}Fe_{0.2}PO_4$, top. The peaks are labeled with the Miller indices of the phospho-olivine structure, *Pnma* spacegroup.

For the case of $LiCoPO_4$, the proposed decomposition reaction is:

$$2LiCoPO_4 \rightarrow Co_2P_2O_7 + Li_2O \quad (2)$$

A similar mechanism leading to the electrochemical formation of Li_2O was reported by Armstrong et al. [12] during the electrochemical charge of Li_2MnO_3:

$$Li_2MnO_3 \rightarrow Li_2O + MnO_2 \quad (3)$$

We believe that Fe^{3+} substitution on the Li^+ and Co^{2+} sites might be a means to slow these types of reactions owing to the higher affinity of Fe^{3+} to oxygen relative to Co^{2+} [13] and/or owing to changes in the underlying electronic structure of Fe^{3+} substituted $LiCoPO_4$ (or substituted $CoPO_4$) relative to pristine $LiCoPO_4$ (or $CoPO_4$).

$LiCoPO_4$ was prepared for comparison to substituted samples. A typical X-ray diffraction pattern is shown as the lower pattern in Fig. 1. The pattern confirms that a single phase $LiCoPO_4$ was prepared. A typical X-ray diffraction pattern is shown as the upper pattern in Fig. 1 for a sample of starting composition $LiCo_{0.8}Fe_{0.2}PO_4$. As with $LiCoPO_4$, there is no evidence of any impurity phases. ICP was used to calculate the amount of Fe^{3+} in the sample of starting composition $LiCo_{0.8}Fe_{0.2}PO_4$ from the assumption that the Fe^{3+} will be compensated by Li^+ ion vacancies. This atomic ratio was measured to be 0.92, which indicate 55% Fe^{2+} and 45% Fe^{3+}. Li^+ is volatilized during the synthesis in order to accommodate the Fe^{3+}. The product for the sample of starting composition $LiCo_{0.8}Fe_{0.2}PO_4$ was thus $Li_{0.92}Co_{0.8}Fe^{2+}_{0.12}\ Fe^{3+}_{0.08}PO_4$ or $Li_{0.92}Co_{0.8}Fe_{0.2}PO_4$, for short. Table 1 shows the lattice constants for the series of compounds prepared for this study.

Fig. 2 demonstrates the effect of Fe substitution on the capacity fade and the importance of the HFiP electrolyte additive. The $Li_{0.92}Co_{0.8}Fe_{0.2}PO_4$ composition was chosen to examine the cycle life since it had the largest capacity at the higher rate. The rate study will be discussed later in the paper. The cells were cycled between 2.5 and 5.3 V via a constant current method at C/5 rate except for the first two cycles which used a C/10 rate. The time of charge was

Table 1
Lattice constants for the series of Fe-substituted $LiCoPO_4$ compounds. Numbers in parentheses are the estimated standard deviation of the last significant digit.

Starting composition	a (Å)	b (Å)	c (Å)	Vol. (Å^3)
$LiCoPO_4$	10.1950(3)	5.9179(1)	4.6972(1)	283.39(1)
$LiCo_{0.95}Fe_{0.05}PO_4$	10.1913(4)	5.9190(2)	4.6983(2)	283.42(2)
$LiCo_{0.9}Fe_{0.1}PO_4$	10.1925(4)	5.9211(2)	4.6991(2)	283.60(2)
$LiCo_{0.8}Fe_{0.2}PO_4$	10.1981(3)	5.9252(1)	4.6986(1)	283.92(1)

also limited to 10 h for C/10 rate and 5 h for C/5 rate so that during the first few cycles the discharge capacity increased after the solid electrolyte interphase (SEI) was formed on the cathode [9].

From Fig. 2, several points can be made. We first, used a standard Li-ion electrolyte (1 m $LiPF_6$ in 3:7 EC:EMC) to compare $LiCoPO_4$ (blue open triangles) to the nominal $Li_{0.92}Co_{0.8}Fe_{0.2}PO_4$ composition (blue open squares). (For interpretation of the references to color in text, the reader is referred to the web version of the article.) For this case, it is clear that the Fe-substituted sample demonstrates considerable improvement in reducing capacity fade. However, capacity fade is still evident. Second, using a high voltage electrolyte (1 m $LiPF_6$ in 3:7 EC:EMC + 1% HFiP additive) we compare the capacity fade of the $Li_{0.92}Co_{0.8}Fe_{0.2}PO_4$ composition (orange solid squares) to the same composition with the standard electrolyte (blue open squares). For this comparison, there is additional decrease of the capacity fade with this change in electrolyte. Third, in order to discriminate fully between the effect of the high voltage electrolyte and the substitutional effects, we compare the $LiCoPO_4$ with standard electrolyte (blue open triangles) to $LiCoPO_4$ with the high voltage electrolyte (orange solid triangles). In this comparison, there is little discernible difference in the fading. Both samples evidence rapid capacity fade. The electrolyte has little effect. Thus, it is clear that structural decomposition of $LiCoPO_4$ or $CoPO_4$ is primarily responsible for the discharge capacity fade of the $LiCoPO_4$ electrode. In quantitative terms, about a 33% drop in capacity is observed between $LiCoPO_4$ (blue open triangles) and nominal $Li_{0.92}Co_{0.8}Fe_{0.2}PO_4$ (blue open circles) at the 10th cycle using a standard electrolyte. The drop in capacity between $LiCo_{0.8}Fe_{0.2}PO_4$ with high voltage electrolyte (orange solid squares) and $Li_{0.92}Co_{0.8}Fe_{0.2}PO_4$ with standard electrolyte (blue open squares) is 12%. Thus, the capacity fade is mainly a result of

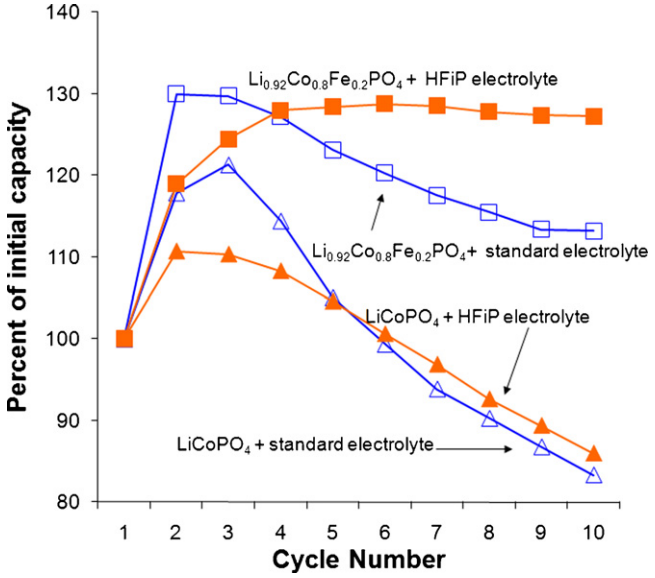

Fig. 2. Effect of $LiCoPO_4$ modification and HFiP electrolyte additive. The "standard (std.) electrolyte" is 1 m $LiPF_6$ in EC:EMC, 3:7. The HFiP electrolyte is 1 m $LiPF_6$ in EC:EMC, 3:7 with 1% HFiP electrolyte additive.

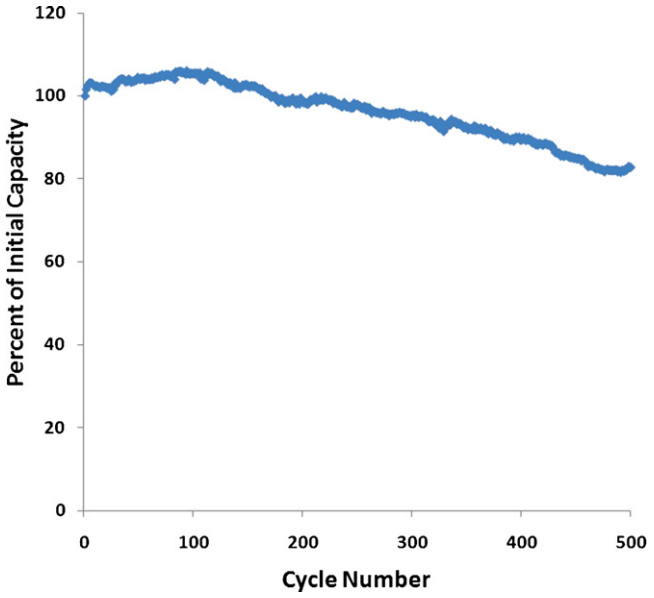

Fig. 3. Long term cycling of composition $Li_{0.92}Co_{0.8}Fe_{0.2}PO_4$ using 1 m $LiPF_6$ in EC:EMC, 3:7 with 1% HFiP electrolyte additive.

$LiCoPO_4/CoPO_4$ structural decomposition and, to a lesser degree, a result of electrolyte decomposition.

Fig. 3 shows the cycling performance of the $Li_{0.92}Co_{0.8}Fe_{0.2}PO_4$ composition over 500 cycles in a coin cell with Li metal as the anode. The coulombic efficiency is about 97%. Although, a noticeable fade is still evident it is a vast improvement over prior literature reports [4–6]. To reiterate, Tadanga et al. [4] observed a 10th cycle discharge capacity of ~52% of the initial capacity, Bramnik et al. [5] reported a 10th cycle discharge of ~59% of the initial capacity and Wolfenstine et al. [6] reported ~53% capacity retention at the 10th cycle. We observe approximately, 100% capacity retention at the 10th cycle and about 80% capacity retention at the 500th cycle. Fig. 4 shows the X-ray diffraction pattern of the cycled nominal $Li_{0.92}Co_{0.8}Fe_{0.2}PO_4$ cathode composite ($Li_{0.92}Co_{0.8}Fe_{0.2}PO_4$ with carbon and PVDF) on Al foil. All peaks can be assigned to the $LiCoPO_4$ olivine structure, indicating structural integrity after cycling of

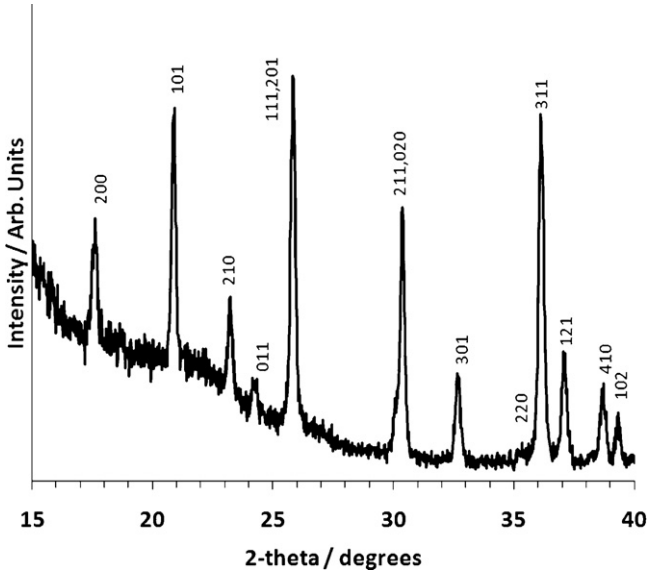

Fig. 4. X-ray diffraction of $Li_{0.92}Co_{0.8}Fe_{0.2}PO_4$ after electrochemical cycling. The peaks are labeled with the Miller indices of the *Pnma*, phospho-olivine structure.

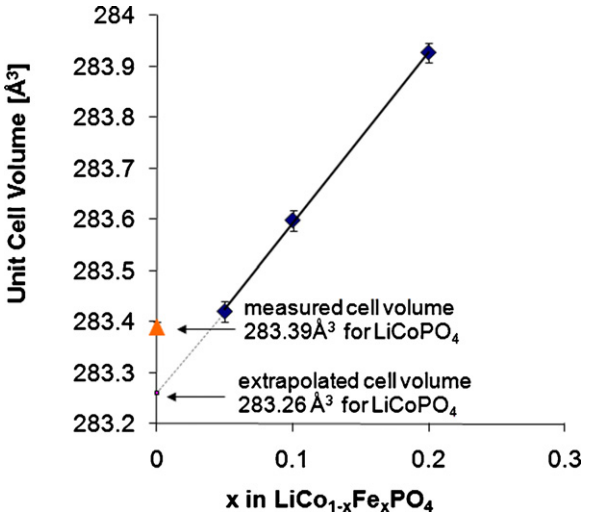

Fig. 5. Unit cell volume as a function of the nominal substitution of Co by Fe in $LiCoPO_4$.

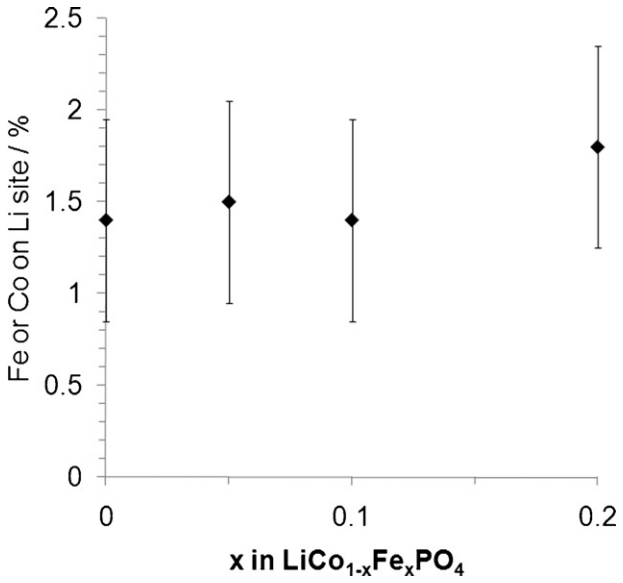

Fig. 6. Percent anti-site disorder on Li site from Rietveld refinement of X-ray diffraction data.

the $Li_{0.92}Co_{0.8}Fe_{0.2}PO_4$ strikingly different from the reported amorphization of $LiCoPO_4$ during cycling [5,6].

Thus, we have shown the improved cycle life of Fe-substituted $LiCoPO_4$ and we assert that it mainly results from the substitution of Fe^{3+} on the Li and Co sites. In order to more fully characterize this substitution we turn to X-ray diffraction, XPS, FTIR spectroscopy and Mössbauer spectroscopy. First, from Rietveld analysis of the X-ray diffraction data, the unit cell volumes of $LiCoPO_4$ and Fe-substituted $LiCoPO_4$ were determined. Fig. 5 shows the effect on unit cell volume by the nominal substitution of Fe for Co^{2+} in $LiCoPO_4$. The observed linear increase in unit cell volume is consistent with the larger unit cell volume of $LiFePO_4$ relative to $LiCoPO_4$. However, the line extrapolated to zero does not intercept at the unit cell volume of Fe free $LiCoPO_4$ as would be expected for $LiCo_{1-d}Fe_dPO_4$ where only Fe^{2+} substitution for Co^{2+} is observed. The "extrapolated volume" is 283.26 Å^3 and the measure volume is 283.39 Å^3. This smaller unit cell volume results from the partial substitution of smaller Fe^{3+} for Li^+ and Co^{2+}.

Rietveld refinements were done to look at the anti-site defects, e.g., Fe^{3+} or Co^{2+} on the Li site. The results are shown in Fig. 6. Hence, this confirms that a small amount of Fe^{3+} is substituting at the Li site ($\sim 1.8 \pm 0.5\%$ for the nominal $LiCo_{0.8}Fe_{0.2}PO_4$ composition). The difference between the Li anti-site defect disorder concentration as a function of Fe content falls within the measurement error. There is on average for all samples about a $1.5 \pm 0.5\%$ concentration of anti-site defects on the Li site. Pujana et al. [14] previously reported the site preference of Fe^{3+} for the Li site in $Li_{1-3x}Fe_xCoPO_4$. They did not report Fe^{3+} substitution on the Co site. This difference from our materials is a result of different starting compositions and different reaction conditions.

Pujana et al. [14] also reported that the infrared (IR) spectra of Fe^{3+} substituted samples have broadened peaks owing to an increase of disorder resulting from the substitution of a portion of the lithium ions by Fe^{3+} and the creation of 2 vacancies per Fe^{3+} atom. The IR spectra of Fe-substituted $LiCoPO_4$ and $LiCoPO_4$ are shown in Fig. 7. We observed a small broadening upon substitution of Li by Fe^{3+}, in agreement with Pujana et al. [14] Furthermore, as additional confirmation of Fe^{3+} in our samples, XPS revealed the presence of both Fe^{2+} and Fe^{3+} in a sample of nominal composition $LiCo_{0.8}Fe_{0.2}PO_4$. Two peaks were observed in the Fe2p spectra which can be assigned to Fe^{3+} and Fe^{2+}.

Mössbauer spectra and analysis were obtained from the SEE Co. (Edina, MN) to corroborate the ICP data with respect to the relative amounts of Fe^{3+} and Fe^{2+} and to learn about the coordination environment of the Fe^{2+} and Fe^{3+}. The room temperature spectrum is shown in Fig. 8. First, we identify the peaks as following: the doublet with the larger splitting (3.0 mm s^{-1}) is typical high spin ($S = 2$) Fe^{2+}. The doublet with the smaller splitting (0.8 mm s^{-1}) and shift (0.44 mm s^{-1}) is typical high spin ($S = 5/2$) Fe^{3+} [14]. Second, the sharpness of the peaks gives information about the local environment. The Fe^{2+} lines are very sharp indicating that Fe^{2+} exclusively sits at one site, the Co site of $LiCoPO_4$ and locally all Fe^{2+} experiences a similar environment [15]. On the other hand, the lines of the Fe^{3+} doublet are broad. The broadening of the peak results from the differences in next nearest neighbors. The M2 (Co) octahedron shares edges with two M1 (Li) octahedra and corners with four M2 octahedra. Thus, the local environment of the M2 site is mainly controlled by the differences in the occupancy of the edge-sharing M1 sites. An Fe^{3+} sited on the M2 will be adjacent to an M1 site containing in order of likelihood either Li^+, a vacancy, or Fe^{3+}. Furthermore, vacant M1 sites will cluster around the Fe^{3+} therefore

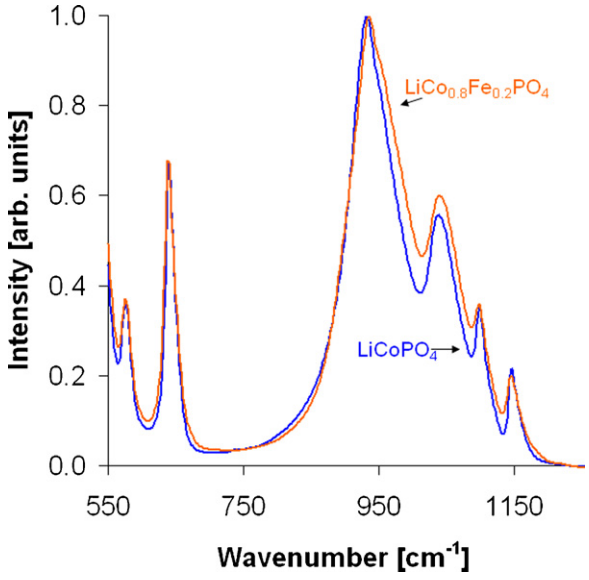

Fig. 7. Comparison of the infrared spectra of samples of nominal composition $Li_{0.92}Co_{0.8}Fe_{0.2}PO_4$ and $LiCoPO_4$.

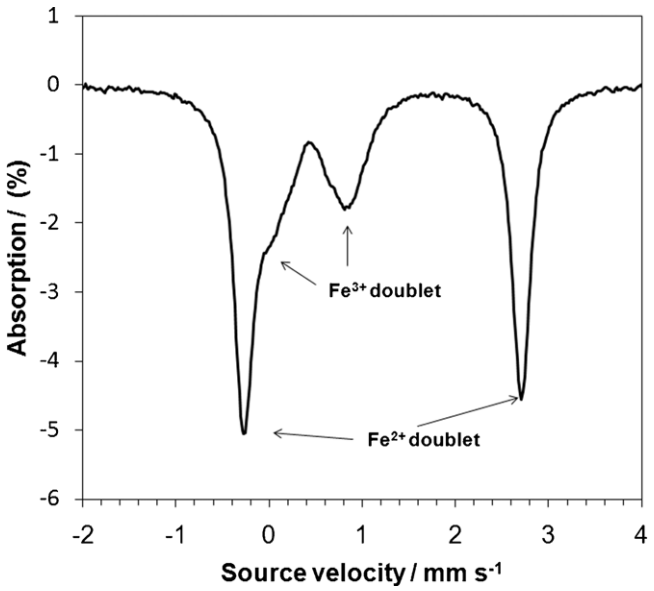

Fig. 8. Mössbauer spectrum of composition $Li_{0.92}Co_{0.8}Fe_{0.2}PO_4$.

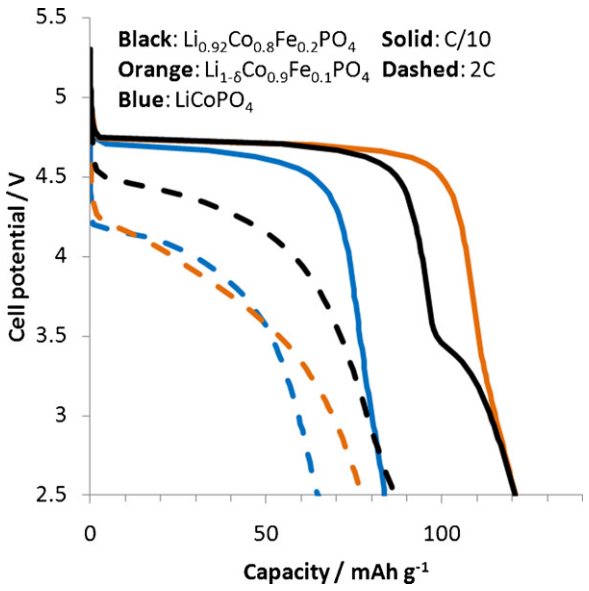

Fig. 9. Discharge curves at different rates for starting compositions, $LiCoPO_4$, $Li_{1-\delta}Co_{0.9}Fe_{0.1}PO_4$, and $Li_{0.92}Co_{0.8}Fe_{0.2}PO_4$.

creating a more heterogenous environment for Fe^{3+} than for Fe^{2+}. Li and Shinno [15] described this "next nearest neighbor effect" in detail for the mineral ferrisicklerite, $Li_{1-x}Mn^{2+}{}_{1-x}Fe^{3+}{}_xPO_4$, a mineral isotypic with the phospho-olivines. Third, from the area of the peaks we can quantify the relative ratio of Fe^{2+}/Fe^{3+}. The Mössbauer spectrum yields 60% Fe^{2+} and 40% Fe^{3+} in excellent agreement with the ICP results. The analysis of the Fe^{2+}/Fe^{3+} ratio by 2 independent methods and 2 different laboratories is summarized in Table 2. All are in excellent agreement.

Finally, having shown the improvements in capacity fade because of the Fe substitution into $LiCoPO_4$, we now show the favorable effects of Fe substitution on capacity as a function of rate in Fig. 9. Typical discharge curves for an electrode of nominal starting composition $LiCoPO_4$ (blue), $Li_{1-\delta}Co_{0.9}Fe_{0.1}PO_4$ (orange) where δ is the Li vacancy concentration and $Li_{0.92}Co_{0.8}Fe_{0.2}PO_4$ (black) are shown. Solid lines represent a C/10 discharge rate and the dashed lines correspond to a 2C discharge rate. Several observations can be noted from Fig. 9. First and foremost, it is clear that Fe-addition improves the capacity at both C/10 and 2C compared to pure $LiCoPO_4$. Second, at the C/10 rate we observe that the nominal $Li_{1-\delta}Co_{0.9}Fe_{0.1}PO_4$ has the longest plateau at 4.8 V. The discharge capacity for the nominal $Li_{0.92}Co_{0.8}Fe_{0.2}PO_4$ is equal, but a portion of the capacity is observed at around 3.5 V, which corresponds to the Fe^{2+}/Fe^{3+} couple. The $LiCoPO_4$ discharge shows evidence of polarization (lower average discharge voltage) compared to the Fe-substituted $LiCoPO_4$. Turning our attention to the 2C discharge curves, we observe that the nominal $Li_{0.92}Co_{0.8}Fe_{0.2}PO_4$ (black dashed curve) has the highest average discharge voltage and the highest capacity. The nominal $Li_{1-\delta}Co_{0.9}Fe_{0.1}PO_4$ and $LiCoPO_4$ have similar discharge voltages though $Li_{1-\delta}Co_{0.9}Fe_{0.1}PO_4$ has a larger capacity. At 2C, the Fe^{3+}/Fe^{2+} plateau is not observed for either Fe containing composition.

The high rate performance may seem surprising owing to the presence of anti-site disorder on the Li site. As discussed previously, the nominal $LiCo_{0.8}Fe_{0.2}PO_4$ composition has about $1.8 \pm 0.5\%$ disorder on the Li site. Intuitively, one would expect that the presence of Fe on the Li site would impede the rate performance by blocking the Li ion channels. However, we postulate that anti-site Fe does not impede the rate for the following reasons. First, the anti-site defect concentration in the Fe substituted samples is not much greater than that reported for typical $LiCoPO_4$ [16]. Second, the anti-site defects will most likely cluster in some fashion. If the defects preferentially occupy certain Li^+ conduction channels they may effectively leave other channels clear to enable Li^+ conduction leading to higher conductivity than if anti-site defects are present in all the channels. The aggregation of defects is a well-known phenomenon. For example, Unger and Perlman [17] showed that divalent impurities in KCl and NaCl form impurity-vacancy dipoles that aggregate in order to form dipolar pairs. The vacancy is a center of excess negative charge and the divalent impurity has an excess positive charge. This creates an electric dipole which will prefer to interact with another dipole in order to collectively lower the energy of the two defects. Similarly, in Fe-substituted $LiCoPO_4$ the $Fe^{\bullet\bullet}_{Li}$ is a center of excess positive and its associated vacancies, V'_{Li}, are centers of excess negative charge and a lower energy state may be achieved by clustering of these defect-vacancy complexes into certain channels leaving other channels free to conduct Li and hence higher conductivity than anti-site defects in all channels. Finally, the rate capability is also a function of the electronic structure and so we further postulate that the rate capability of the Fe-substituted $LiCoPO_4$ is enhanced relative to pristine $LiCoPO_4$ because of the substitution of Fe for Co.

Table 2
Analysis of the Fe^{3+} content for sample of starting composition $LiFe_{0.2}Co_{0.8}PO_4$.

Analysis method	Atom % Fe^{2+} of total Fe	Atom % Fe^{3+} of total Fe	Laboratory
Mössbauer	60	40	SEE Co.
ICP-OES (from Li/M)	55	45	Galbraith Laboratories, Inc.
Average	~58	~42	

4. Conclusion

A synthesis method for Fe-substituted $LiCoPO_4$ electrode material has been reported. The improved rate and dramatically reduced capacity fade is striking. The capacity fade of $LiCoPO_4$ results mainly from structural decomposition of $LiCoPO_4/CoPO_4$ and to a lesser degree results from electrolyte decomposition. Fe^{3+} on the Li and Co sites appears to stabilize the structure. X-ray diffraction, XPS, Mössbauer Spectroscopy, ICP-OES and FTIR spectroscopy confirm the presence of Fe^{3+} on the Li and Fe^{3+}/Fe^{2+} on the Co sites. Use of the HFiP containing electrolyte further reduced capacity fade during charge–discharge cycling of the Fe-substituted-$LiCoPO_4$. This Fe-substitution in combination with the HFiP containing electrolyte shows dramatically improved discharge capacity retention as well as improved rate capability relative to un-substituted $LiCoPO_4$ with "standard" Li-ion electrolyte.

Acknowledgements

We thank ARL colleagues Kang Xu and Arthur von Cresce for providing electrolyte, Unchul Lee for XPS measurements and Bruce Poese for obtaining FT-IR spectra. We thank Thomas Kent (SEE Co.) for obtaining and assisting with the analysis of the Mössbauer spectrum.

References

[1] A.K. Padhi, K.S. Nanjundaswamy, J.B. Goodenough, J. Electrochem. Soc. 144 (1997) 1188.
[2] K. Amine, H. Yasuda, M. Yamachi, Electrochem. Solid State Lett. 3 (2000) 178.
[3] J. Wolfenstine, J.L. Allen, J. Power Sources 142 (2005) 389.
[4] K. Tadanaga, F. Mizuno, A. Hayashi, T. Minami, M. Tatsumisago, Electrochemistry 71 (2003) 1192.
[5] N.N. Bramnik, K.G. Bramnik, T. Buhrmester, C. Baehtz, H. Ehrenberg, H. Fuess, J. Solid State Electrochem. 8 (2004) 558.
[6] J. Wolfenstine, U. Lee, B. Poese, J.L. Allen, J. Power Sources 144 (2005) 226.
[7] J. Wolfenstine, J. Read, J.L. Allen, J. Power Sources 163 (2007) 1070.
[8] J. Wolfenstine, J.L. Allen, J. Power Sources 136 (2004) 150.
[9] A.V. Cresce, K. Xu, J. Electrochem. Soc. 158 (2011) A337.
[10] M.E. Rabanal, M.C. Gutierrez, F. Garcia-Alvarado, E.C. Gonzalo, M.E. Arroyo-de Dompablo, J. Power Sources 160 (2006) 523.
[11] N.N. Bramnik, K. Nikolowski, D.M. Trots, H.E. Bramnik, Electrochem. Solid-State Lett. 11 (2008) A89.
[12] A.R. Armstrong, M. Holzapfel, P. Novak, C.S. Johnson, S.H. Kang, M.M. Thackeray, P.G. Bruce, J. Am. Chem. Soc. 128 (2006) 8694.
[13] R.H. Perry, D.W. Green, J.O. Maloney (Eds.), Perry's Chemical Engineers' Handbook, sixth ed., McGraw-Hill Book Company, New York, 1984, p. 3-149.
[14] A. Pujana, J.L. Pizzarro, A.A. Goni, T. Rojo, M.I. Arriortua, Anal. Quim. Int. Ed. 94 (1998) 383.
[15] Z. Li, I. Shinno, Miner. J. 19 (1997) 99.
[16] S. Adams, J. Solid State Electrochem. 14 (2010) 1787.
[17] S. Unger, M.M. Perlman, Phys. Rev. B 10 (1974) 3692.